Astronomy Reports, Vol. 41, No. 1, 1997, pp. 19–27. Translated from Astronomicheskii Zhurnal, Vol. 74, No. 1, 1997, pp. 25–33.

The Observational Manifestations of HI Shells in Different Velocity Channels

S. Ya. Mashchenko and S. A. Silich

Main Astronomical Observatory, National Academy of Sciences of Ukraine, Goloseevo, Kiev, 252127 Ukraine

Received March 14, 1996

Abstract—This paper describes an algorithm making it possible to construct images of three-dimensional supershells of neutral hydrogen in the plane of the sky in different velocity channels. A broadening of the 21-cm line due to chaotic motions in the gas and the finite angular resolution of the radio telescope are taken into account. Taking account of the broadening of the spectral line proves to be of fundamental importance in modeling observations of shells. Criteria usually applied in the preparation of catalogs of regions deficient in HI in nearby galaxies are analyzed, using several model supershells for the galaxies M31 and HoII as examples. It is shown that three of these criteria—the observation of a "hole" in no fewer than three neighboring velocity channels, immobility of the center of the "hole," and a sharp contrast between the "hole" and the background in all relevant channels—are well satisfied for supershells located close to the galactic node line, and are more poorly satisfied for supershells located far from it.

1. INTRODUCTION

This paper continues a series of articles dedicated to the development of numerical models for the creation and evolution of giant expanding shells of interstellar gas [1–7]. Numerical schemes based on the thin layer approximation [1, 8, 9] have proved to be especially fruitful in the study of the morphology and dynamics of these complex three-dimensional objects, which arise through the collective action of supernovae concentrated in a modest spatial region on the surrounding gas. The development of these schemes and the addition of complexities to them makes it possible, in our opinion, to turn from a discussion of the main characteristics of the phenomenon under consideration to a more detailed comparison of theoretical models and observational data at radio and other wavelengths. In [6, 7], we developed a procedure for projecting three-dimensional shells, making it possible to calculate maps of the HI surface density distribution in the plane of the sky and to take into account the effects of projection on the shell "image." The study of a number of details in the behavior of the shells (their expansion velocities, identification against the general galactic background, etc.) requires modeling of "images" of these objects at different frequencies and comparing these models with observations. The extreme complexity of the observed distribution of neutral hydrogen made clear the necessity of developing a set of intuitively clear criteria permitting identification of real regions deficient in HI against the general galactic background with maximum certainty; these criteria should operate under conditions of insufficient resolution and a relatively high noise level. As a rule, the following four criteria are used in the analysis of observational data:

(1) The HI hole should be clearly visible in no fewer than three consecutive velocity channels.

(2) The center of the hole should not move spatially in any of these channels.

(3) There should be a clear contrast between the region deficient in HI and the surrounding gas in the relevant channels.

(4) The shape of the hole should be close to elliptical.

These criteria were applied to the galaxy M31 in [10]. Deul and den Hartog [11] used these same criteria to compose a catalog of holes in the galaxy M33. A somewhat less strict set of criteria (3 and 4) was applied to the galaxy HoII in [12].

The selection criteria presented above do not have a rigorous basis, but rather are founded on intuitive concepts about how an expanding shell should appear. In this paper, we analyze them from the point of view of our results of numerical modeling of shell evolution. Apart from the projection procedure described in [7], we develop a procedure for constructing maps of the column density of HI in different velocity channels, taking the spatial resolution of the radio telescope into account. We will show below that, in this analysis, a fundamental role is played by the chaotic motions of the interstellar gas. We will also consider the role of the criteria listed above in the identification of real objects. Section 2 describes the algorithm for the projection of three-dimensional shells onto the plane of the sky in different velocity channels. In Section 3, we discuss the observational manifestation of numerically projected supershells in models for the galaxies M31 and HoII. In Section 4, we formulate the main results of this work.

1063-7729/97/4101-0019$10.00 © 1997 МАИК Наука/Interperiodica Publishing

2. THE NUMERICAL SCHEME

We used the algorithm described in [2, 3, 6], based on the thin layer approximation, in modeling the evolution of supershells. We used the models for the galaxies HoII and M31 described in [7]. We have modified the procedure for projecting the shells onto the plane of the sky so that it is possible to obtain the distribution of the column density of HI in different velocity channels instead of the integrated HI concentration distribution.

For an optically thin layer of neutral hydrogen in thermodynamic equilibrium, the column density of HI atoms is directly proportional to the brightness temperature of the gas [13]. We will therefore work directly with the number of atoms along the line of sight, which is found straightforwardly from the numerical model. We may write the number of atoms of neutral hydrogen in a column of unit cross section along the line of sight with radial velocity in a unit velocity interval around U, allowing for chaotic motions in the interstellar medium, in the form

$$N(U) = \frac{1}{\sigma_g\sqrt{2\pi}}\int_{-\infty}^{\infty} n(z')\exp\left\{-\frac{1}{2}\left[\frac{V(z')-U}{\sigma_g}\right]^2\right\}dz'. \quad (1)$$

Here, (x', y', z') is a coordinate system fixed to the plane of the sky (the Z' axis is oriented along the line of sight toward the observer); $V(z')$ and $n(z')$ are the radial velocity and number density of the gas; and σ_g is the one-dimensional velocity dispersion for chaotic motions of the HI, taking account of the contribution of both turbulent and thermal motions of the neutral hydrogen atoms. We assume here that σ_g is constant along the line of sight.

Let there be given a set of spectral filters with a normalized sensitivity curve $W_j(U), j = 1, 2, 3, \ldots$, where j numbers consecutive channels. In this case, we may express the column density of HI atoms in an arbitrary spectral (velocity) channel in the form

$$N_j = \int_{-\infty}^{\infty} N(U)W_j(U)dU. \quad (2)$$

The sensitivity curve for the spectral filters is given in the form of a gaussian with dispersion σ_f:

$$W_j(U, \sigma_f) = \frac{1}{\sigma_f\sqrt{2\pi}}\exp\left\{-\frac{1}{2}\left[\frac{U-V_j}{\sigma_f}\right]^2\right\}, \quad (3)$$

where the V_j are the central velocities for the corresponding filters. After substituting (1) and (3) into (2) and integrating the resulting expression over U, we obtain a formula for the column density of HI in the jth channel:

$$N_j = \frac{1}{\sigma_*\sqrt{2\pi}}\int_{-\infty}^{\infty} n(z')\exp\left\{-\frac{1}{2}\left[\frac{V(z')-V_j}{\sigma_*}\right]^2\right\}dz', \quad (4)$$

where we have introduced the notation

$$\sigma_* = \sqrt{\sigma_f^2 + \sigma_g^2}. \quad (5)$$

We may write the total column density of HI atoms in the jth channel, allowing for the contribution of quiescent gas and elements of the supershell, in the form

$$N_j(x', y') = \sum_l N_l W_j(V_l, \sigma_f) + \int_{-\infty}^{\infty} n(x', y', z')W_j[V(x', y', z'), \sigma_*]dz', \quad (6)$$

where we have taken account of the fact that the velocity dispersion in the cold dense shell σ_{sh} is substantially smaller than the width of the spectral filter, $\sigma_{sh} \ll \sigma_f$. The index l numbers the shell elements intersected by the line of sight, N_l is the contribution of each element to the total column density in the spherical segment approximation [7], and V_l is the radial velocity of the corresponding element.

Formula (6) shows that observations of interstellar gas allowing for chaotic motions ($\sigma_g \neq 0$) are equivalent to observations of HI with zero velocity dispersion, but with a wider filter—with half-width σ_* rather than σ_f. In the case of very large chaotic motions ($\sigma_g \longrightarrow \infty$), modeling the results for different velocity channels becomes identical to modeling the integrated number of atoms along the line of sight. It follows from formula (6), however, that this is true only for the quiescent gas. The contributions of shell elements in different velocity channels are always different.

In order to allow for the finite spatial resolution of the radio telescope, the distribution of the column density of HI obtained from (6) must be smoothed:

$$N_{\mathrm{sm},j}(x', y') = \iint N_j(x'', y'')F\left(\sqrt{(x'-x'')^2 + (y'-y'')^2}\right)dx''dy''. \quad (7)$$

Here, $F(r)$ is the smoothing function, r is the distance from the point at which we calculate the column density to an arbitrary point in the plane of the sky, and $N_{\mathrm{sm},j}(x', y')$ is the smoothed value of the column density in the jth velocity channel. The integration is conducted over the entire region considered. We have used a

spherical two-dimensional gaussian as a smoothing function (see, for example, [14]):

$$F(r) = \frac{1}{2\pi\sigma_b^2}\exp\left(-\frac{r^2}{2\sigma_b^2}\right), \quad (8)$$

where σ_b is the dispersion of this gaussian. The resolution of the radio telescope is usually characterized by the full width at half maximum (FWHM) intensity of the beam. Using (8), we may express σ_b in terms of the FWHM:

$$\sigma_b = \frac{\mathrm{FWHM}}{2\sqrt{2\ln 2}}. \quad (9)$$

3. CALCULATION RESULTS

We considered two cases of supershell evolution: in the galaxy M31, with an energy source with power $L = 10^{38}$ erg s^{-1} at a distance of 10 kpc from the center, and in the galaxy HoII (UGC 4305), with an energy input rate to a cavity of $L = 10^{37}$ erg s^{-1} at a distance $R = 4$ kpc from the center of the galaxy. The energy source was turned off after 30 Ma, and we assumed that by this time all massive stars in OB associations had exploded as supernovae. The shells were projected onto the plane of the sky in different velocity channels after 25 Ma of evolution in M31 and 40 Ma of evolution in HoII, taking account of the finite angular resolution of the radio telescope [see (7)]. We chose the distance between the centers of channels ΔV to be the same as in [10, 12]: $\Delta V = 8.2$ km s^{-1} for M31, and $\Delta V = 2.58$ km s^{-1} for HoII. The half-width of the filters σ_f was assumed to be equal to half the spectral resolution. For M31 and HoII, $\sigma_f = 4.1$ and 1.29 km s^{-1}, respectively. Taking account of the FWHM of the telescope beam, equal to 100 pc for M31 and 66 pc for HoII, the dispersions of the spherical gaussian of the beam core σ_b (9) are equal to 42.3 and 28 pc, respectively. The one-dimensional dispersions for the chaotic gas velocities σ_g were taken to be 8.1 km s^{-1} for M31 [15] and 6.8 km s^{-1} for HoII [12]. The image of a shell in the plane of the sky depends on the polar angle θ of the parent OB association (which is measured from the node line of the galaxy); this dependence is more pronounced for galaxies with large inclination angles. We therefore carried out the projections for several angles θ: 0°, 30°, 60°, and 90° for M31 and 0°, 45°, and 90° for HoII.

Figures 1 and 2 show calculated maps of the distribution of the column density $N_{\mathrm{sm},j}$ for supershells in M31 and HoII. The velocity channels in which the hole has the highest contrast are indicated in the figures. When the HI hole is not observed, the channel corresponding to the radial velocity of the shell center is shown. We calculated each projection both without taking account of chaotic motions in the interstellar gas [$\sigma_g = 0$ in formula (5)] and taking account of the broadenning of the HI spectral line due to turbulent and thermal motions of the atoms ($\sigma_g = 8.1$ km s^{-1} for M31 and 6.8 km s^{-1} for HoII). Three levels are shown in the maps of column density $N_{\mathrm{sm},j}$ for holes in the HI distribution: the minimum and maximum levels giving closed contours $N_{\min}$ and $N_{\max}$ (thin lines), and a level corresponding to half the depth of the hole $N_{50\%} = (N_{\min} + N_{\max})/2$ (thick line). Analogous to [10, 12], the level $N_{50\%}$ is identified with the hole boundary.

The distribution of the column density in the velocity channels for M31 shown in Fig. 1 leads us to conclude that taking account of chaotic motions in the interstellar gas is of fundamental importance. It is clear from Fig. 1 that there is not a single closed contour for the case $\sigma_g = 0$ (left panels) for the polar angles $\theta = 30°$, 60°, and 90°; i.e., the shell does not manifest itself as a hole in the HI distribution in any of the velocity channels. The effect of chaotic motions on the appearance of the shell may be neglected only for polar angles close to 0°. This effect is explained by the fact that, when $\sigma_g = 0$, the width of the region corresponding to quiescent gas in the maps of the distribution of column density $N_{\mathrm{sm},j}$ is smaller than the size of the hole. The effect of this on the possibility of detecting the shell observationally is discussed in [10]. For $\theta = 0°$, the quiescent gas occupies a rather wide band, even without allowing for the broadenning of the HI spectral line due to thermal and turbulent gas motions.

In the case of HoII (Fig. 2), the chaotic motion of the interstellar gas exerts a significant influence on the appearance of the shell only for polar angles $45° \le \theta \le 90°$. Even for $\theta = 90°$ in the case $\sigma_g = 0$, however, we observe closed contours in the distribution of column density $N_{\mathrm{sm},j}$.

We note a "two-humped" character in the spectrum for many holes observed in the galaxy HoII (Fig. 10 of [12], for example). This has been interpreted as contributions to the total spectrum of the approaching and receding shell walls [12]. Figure 3 shows theoretical, calculated "spectra" for a supershell in HoII, located on the node line ($\theta = 0°$) at a distance of $R = 4$ kpc from the center (these coordinates are close to those for observed hole 35 in the list of [12]). Spectra calculated for the cases (a) $\sigma_g = 0$ and (b) $\sigma_b = 6.8$ km s^{-1} are shown. It is clear from this figure that the "two-humped" character is seen when the chaotic gas motions are taken into consideration (Fig. 3b), but not in the case $\sigma_g = 0$ (Fig. 3a). This is because when the broadening of the spectral line is not taken into account, the relative column density of quiescent gas atoms in a given channel in the shell region is greater than in the case when σ_g differs from zero. This leads to a sharp decrease in the relative contribution of the shell to the total column density. Thus, allowing for chaotic motions in the interstellar gas is important when comparing the numerical modeling results for HoII with the observational data.

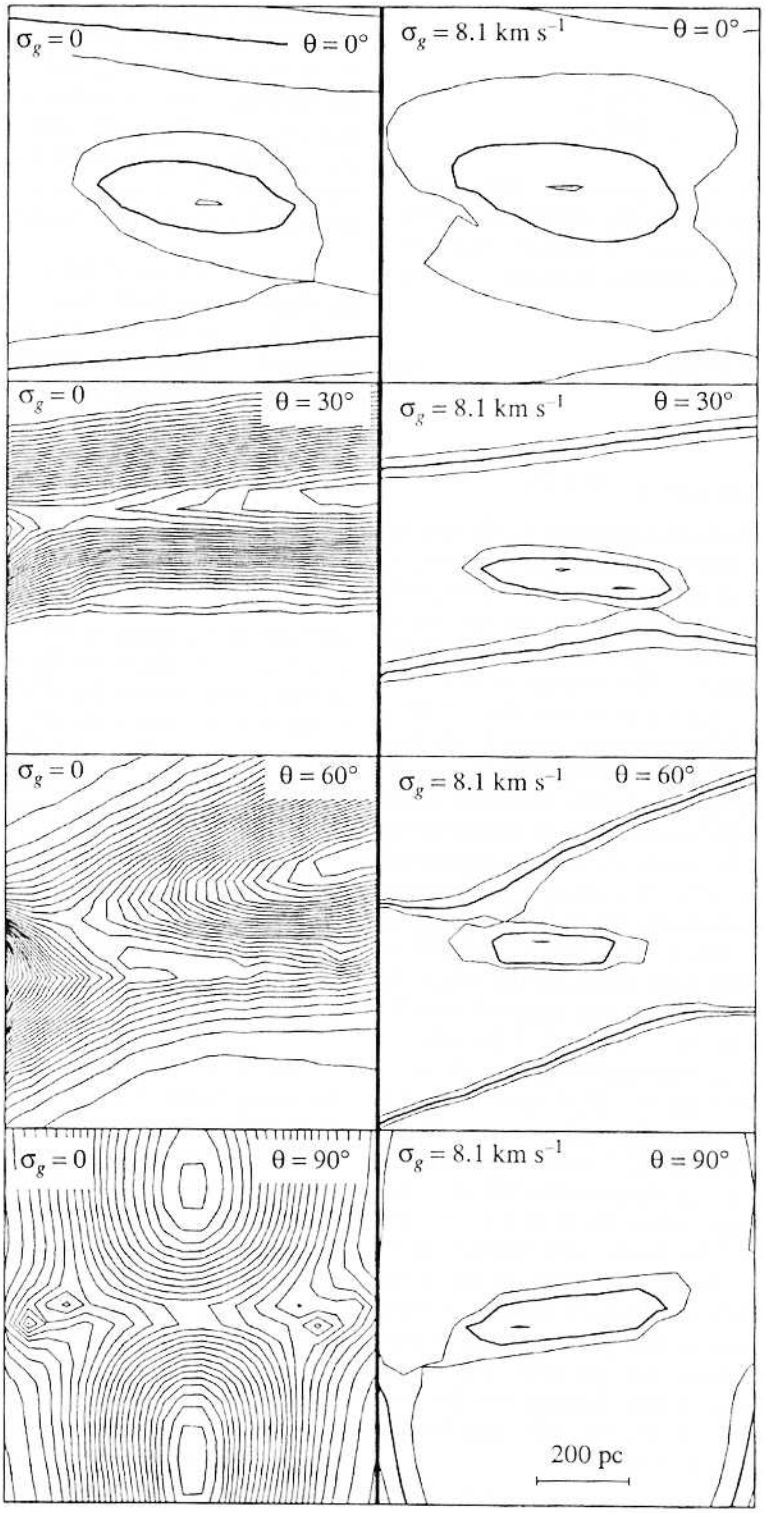

Fig. 1. Distribution of the column density $N_{\mathrm{sm},j}$ for supershells in the galaxy M31 with different polar angles for two values for the chaotic velocity dispersion in the gas: $\sigma_g = 0$ and $\sigma_g = 8.1$ km s^{-1} (see text for a fuller explanation).

The calculated characteristics of the holes in the distribution of neutral hydrogen in different velocity channels and for different polar angles for the galaxies M31 and HoII are presented in Tables 1 and 2. Here, Δj is the distance of the jth channel from the central channel in units of ΔV; V_j^* is the radial velocity corresponding to the center of the given velocity channel (in which the systematic motion of the galaxy V_{sys} is taken into

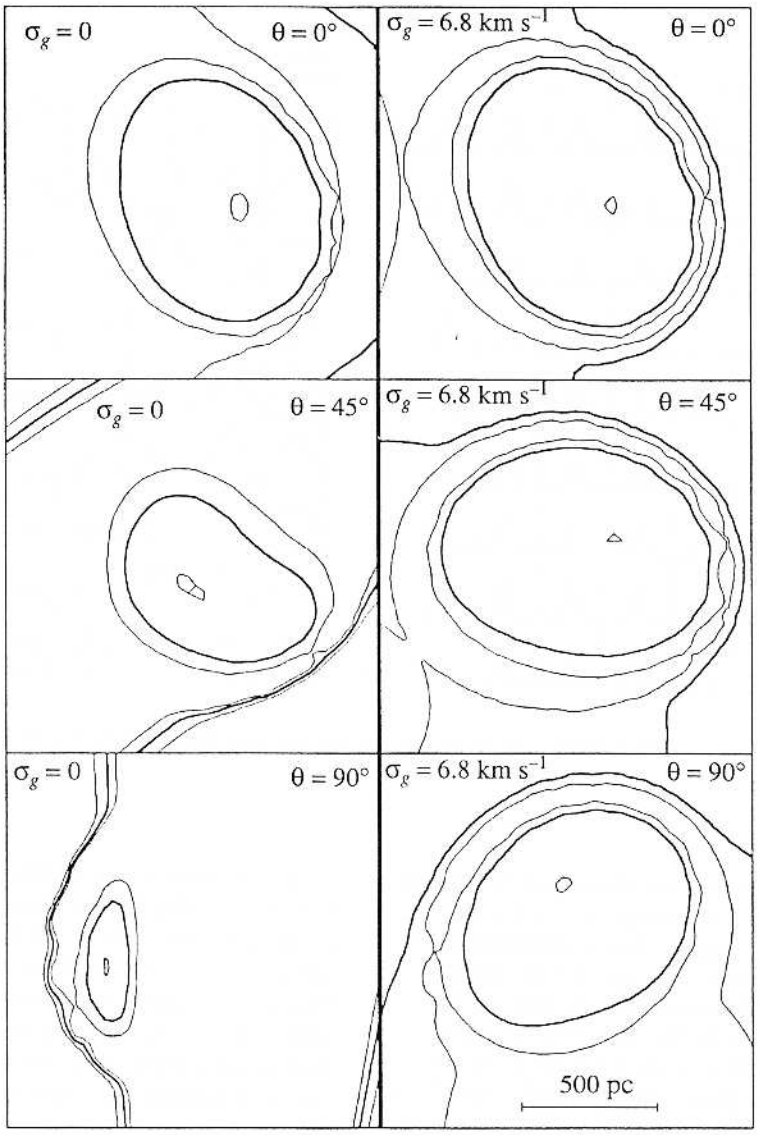

Fig. 2. Distribution of the column density $N_{sm,j}$ for supershells in the galaxy HoII with different polar angles for two values for the chaotic velocity dispersion in the gas: $\sigma_g = 0$ and $\sigma_g = 6.8$ km s^{-1} (see text for a fuller explanation).

account; $V_{sys} = -315$ km s^{-1} for M31 [16] and 157 km s^{-1} for HoII [12]). X_0' and Y_0' are coordinates of the center of the ellipse approximating the hole at the level $N_{50\%}$, in the plane of the sky in a coordinate system with the origin at the center of the galaxy and the X' axis along the node line of the galaxy; DIAM is the diameter of this ellipse, equal to $\sqrt{ab}$, where a and b are the major and minor axes of the ellipse. $\xi = (N_{max} - N_{min})/N_{50\%}$ is the hole contrast, and Δ is the distance of the hole center in the current channel from the hole center in the central channel for the given polar angle.

Tables 1 and 2 show that the hole center in different velocity channels may shift over a significant distance, which may be comparable to the hole diameter. This is expressed most clearly for shells located close to the node line (with the polar angle $\theta > 0°$). The diagram in Fig. 4 offers a qualitative explanation of this. Let us suppose that the observer is located in the plane of the galaxy and observes the distribution of neutral hydrogen in very narrow velocity channels. Let the gas in the galaxy be distributed uniformly, and the rotational velocity not depend on distance from the galactic center: $n(x, y) \equiv$ const, $V(x, y) \equiv$ const. In this case, in each channel, gas located along some radius vector is observed (see the lines of sight l_1 and l_2 in Fig. 4). Thus, radius vectors with different polar angles correspond to different velocity channels. The hole in the HI distribution will be observed in those channels

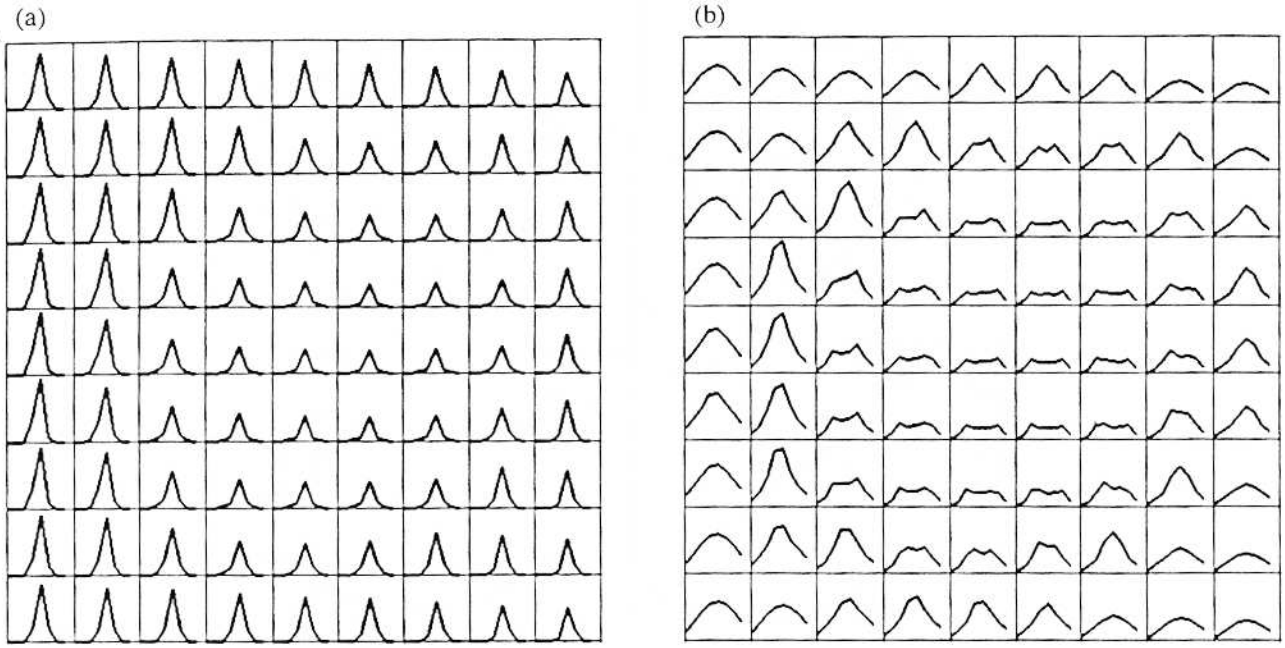

Fig. 3. Schematic maps of the calculated profiles of the HI spectral line near the supershell in the galaxy HoII: (a) $\sigma_g = 0$ and (b) $\sigma_g = 6.8$ km s^{-1}.

corresponding to radius vectors that intersect the cavity from which gas has been swept out. It is clear from the diagram that, if the region that is deficient in neutral hydrogen is close to polar angle $\theta = 0°$, the centers of the "hole" in the observed distribution of column density will nearly coincide for all velocity channels in which these "holes" are observed (zone B in the diagram). For shells with polar angles $\theta \neq 0°$, the "hole" centers in different velocity channels will be systematically shifted. In the limiting case $\theta = 90°$ (Fig. 4), the observed "holes" in the edge channels are located so far from each other (zones A_1 and A_2) that there is no overlap between them.

This diagram does not take into account the contribution of the shell walls to the column density. In the edge velocity channels in which the hole is still observed, however (it is precisely in these channels that the shift of the hole center should be most strongly seen), the contribution of the shell elements becomes substantially smaller than that of the quiescent gas. This is because the velocity dispersion (and the line width) in the cold dense shell is significantly smaller than in the surrounding interstellar gas. The diagram in Fig. 4 illustrates the limiting case of the galactic inclination angle $i = 90°$. Qualitatively, it makes sense that the shift of the hole center should decrease with a decrease in the inclination i, and for the opposite limiting case $i = 0°$ this shift should approach zero.

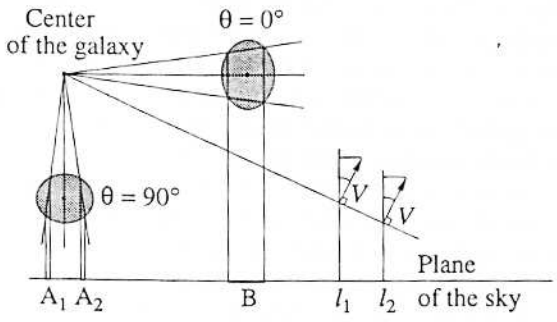

Fig. 4. Diagram illustrating the shift of the HI hole center in different velocity channels (see text for a fuller explanation).

Figure 5 shows the shift in the hole centers in different velocity channels from our calculations for M31 and HoII. Figure 5a shows the results of calculations for shells in M31 at a distance of $R = 10$ kpc from the center, with the polar angle $\theta = 30°$. Figure 5b shows the calculation results for shells in HoII; the center of the shell is at a distance of $R = 4$ kpc from the center of the galaxy, and $\theta = 45°$. In each figure, the images for the holes in three velocity channels—the channel in which the hole diameter is largest, and the limiting channels in which the hole can still be distinguished—are overlaid. The thick line denotes the contour corresponding to the central channel, while the thin lines denote those corresponding to the two limiting channels. It is clear from these figures that the shift in the hole center in different channels can be significant, and can even approach the observed diameter of the hole. The images for the same hole in the limiting

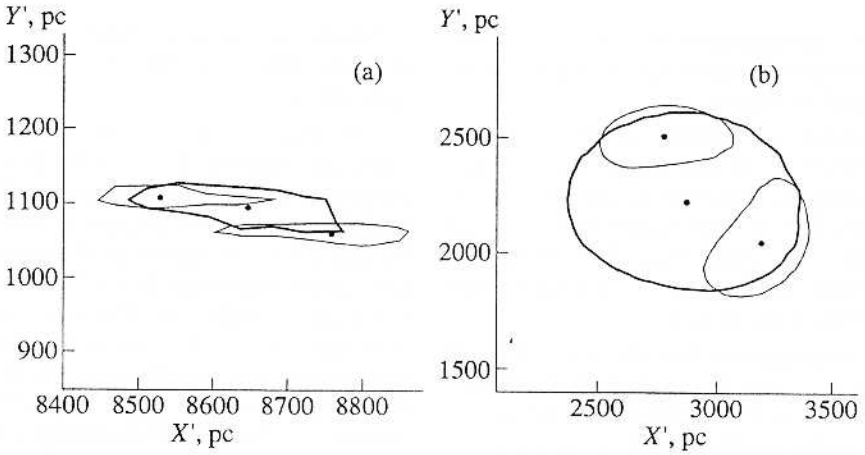

Fig. 5. Position of the hole center in different channels for the supershells in (a) M31 and (b) HoII (see text for a fuller explanation).

channels are so distant from each other that they virtually do not overlap.

Of course, Fig. 5 shows a limiting, idealized case. In the edge channels, the contrast of the hole sharply decreases (Tables 1, 2), and it may be difficult to distinguish it against the background of the surrounding gas. Nonetheless, the variation of the position of the hole center in different channels indicated by the calculations

Table 1. Characteristics of calculated HI holes in different velocity channels for the Galaxy M31

Δj	V_j^*, km s^{-1}	X_0', pc	Y_0', pc	DIAM, pc	$N_{50\%}$, 10^{12} s cm^{-3}	ξ	Δ, pc
			$\theta = 0°$				
−5	−573.3	10055	−6	254	23	0.54	50
−4	−569.2	10071	−13	249	69	0.53	67
−3	−565.1	10070	−26	245	174	0.46	68
−2	−561.0	10024	−33	242	349	0.47	35
−1	−556.9	10000	−25	245	545	0.59	21
0	−552.8	10005	−4	280	717	0.67	0
1	−548.7	10010	17	316	801	0.73	22
2	−544.6	9989	28	321	696	0.69	36
3	−540.5	9946	19	328	470	0.63	63
4	−536.4	9944	7	327	263	0.59	62
5	−532.3	9945	3	314	128	0.52	61
			$\theta = 30°$				
−2	−528.2	8531	1108	82	347	0.10	112
−1	−524.1	8585	1100	102	442	0.14	58
0	−520.0	8643	1095	121	464	0.13	0
1	−515.9	8686	1086	185	495	0.21	45
2	−511.8	8761	1058	89	362	0.10	124
			$\theta = 60°$				
−1	−438.0	4929	1885	81	438	0.07	63
0	−433.9	4992	1880	153	466	0.15	0
1	−429.8	5031	1877	183	482	0.11	39
			$\theta = 90°$				
0	−315.0	1	2167	211	598	0.29	0

Table 2. Characteristics of calculated HI holes in different velocity channels for the Galaxy HoII

Δj	V_j^*, km s^{-1}	X_0', pc	Y_0', pc	DIAM, pc	$N_{50\%}$, 10^{12} s cm^{-3}	ξ	Δ, pc
			$\theta = 0°$				
−4	122.1	4164	−41	706	90	0.41	106
−3	124.7	4225	−52	663	152	0.35	168
−2	127.3	4446	−144	321	239	0.15	406
−1	129.9	4046	−34	698	321	0.68	26
0	132.4	4061	−13	881	433	1.00	0
1	135.0	4117	−16	720	355	0.82	56
2	137.6	4169	−12	304	261	0.14	108
3	140.2	4122	−25	793	164	0.35	62
			$\theta = 45°$				
−3	132.4	2785	2503	386	150	0.17	298
−2	135.0	2950	2196	258	294	0.08	76
−1	137.6	2916	2187	802	377	0.77	51
0	140.2	2878	2220	874	417	0.92	0
1	142.8	2938	2290	351	280	0.20	92
2	145.3	3197	2045	451	174	0.23	364
			$\theta = 90°$				
−2	150.5	−380	3130	303	148	0.15	418
−1	153.1	65	3168	459	273	0.33	34
0	155.7	37	3149	801	366	0.73	0
1	158.2	−12	3185	684	321	0.56	61
2	160.8	−32	3219	274	268	0.10	98

must be taken into consideration when interpreting observations and composing catalogs of regions that are deficient in neutral hydrogen.

Figures 1 and 2 show that another criterion—closeness of the shape of the hole to that of an ellipse (criterion 4)—is satisfactorily fulfilled for all calculated projections of supershells both for M31 and for HoII. In all the maps presented, the level $N_{50\%}$ describing the boundary of the observed hole is a bulging closed curve, well approximated by an ellipse.

Criterion 1—the requirement that the hole in the HI distribution be observed in no fewer than three consecutive velocity channels—is not fulfilled only for supershells in M31 with polar angles $\theta = 90°$ (Tables 1, 2). We note a general tendency in both galaxies for a decrease in the number of channels in which the holes are observed as the polar angle is varied from $\theta = 0°$ to 90°. This effect is more strongly manifested in galaxies with larger inclination angles. In M31, the number of channels decreases from 11 (for $\theta = 0°$) to 1 (for $\theta = 90°$). For HoII, the effect is less significant—the number of channels decreases from 8 to 5.

If we take account of the fact that the maximum contrast of a hole for a given polar angle as a rule decreases with distance of the supershell from the node line (Tables 1, 2), we conclude that three of the selection criteria usually applied—observation of the hole in no fewer than three channels, immobility of the hole center in each channel, and a sufficiently sharp hole contrast (criteria 1, 2, and 3)—best describe real supershells located close to the galactic node line. In the transition to polar angles close to $\theta = 90°$, identifying analogous objects by these three observational criteria is substantially more difficult.

We have studied here the observational manifestations of isolated supershells. The density of shells in the central regions of irregular galaxies [12] and the possibility of overlapping between these objects in very inclined galaxies may make identification of real shells in these systems more difficult.

4. CONCLUSION

In conclusion, we present the main results of this paper.

(1) We have constructed an algorithm permitting us to obtain maps of the distribution of the column density of HI in different velocity channels. Account is taken of the finite angular resolution of the radio telescope and of chaotic motions in the interstellar medium. The algorithm developed makes it possible to compare directly numerical models of the evolution of three-dimensional shells with radio astronomical observations.

(2) Using several supershells in the galaxies M31 and HoII as examples, we have shown the fundamental importance of allowing for broadening of the HI 21-cm line due to chaotic motions of the quiescent gas in modeling the observational manifestations of shells (the presence of closed contours in the distribution of the column density in velocity channels, "two-humped" spectral lines).

(3) Analysis of our theoretically calculated projections of supershells reveals that the center of the observed hole in the distribution of HI should be shifted in different velocity channels. This is primarily caused by the effect of differential rotation of the quiescent gas, and is more significant for supershells located near the galactic node line. The total shift in the edge channels may exceed the size of the hole in these channels, and may be comparable with the diameter of the hole in the central channel. In the edge channels, however, the contrast of the hole drops sharply, making it more difficult to distinguish the hole against the background of the surrounding gas.

(4) Our numerical calculations for individual shells in M31 and HoII show that three of the four criteria usually applied in the analysis of radio astronomical data for the selection of regions deficient in HI are well satisfied by supershells located close to the galactic node line; these criteria are observation of the hole in no fewer than three consecutive velocity channels, immobility of the hole center in each relevant channel, and sufficiently high contrast for the hole. Their applicability worsens in the transition to polar angles close to $\theta = 90°$. Identification of supershells using these criteria in this case becomes significantly more difficult. The fourth observational criteria (closeness of the shape of the hole boundary to elliptical) is satisfactorily fulfilled in all examples considered here.

ACKNOWLEDGMENTS

This work was partially supported by the International Science Foundation (grant no. UC 9000) and by the United Foundation of the Ukrainian Government and the International Science Foundation (grant no. UC 9200). S.Ya. Mashchenko thanks the International Soros Scientific Educational Program for partial support (grant no. PSU 052088).

REFERENCES

1. Bisnovatyi-Kogan, G.S., Blinnikov, S.I., and Silich, S.A., *Astrophys. Space Sci.*, 1989, vol. 154, p. 229.
2. Bisnovatyi-Kogan, G.S. and Silich, S.A., *Astron. Zh.*, 1991, vol. 68, p. 749.
3. Silich, S.A., *Astrophys. Space Sci.*, 1992, vol. 195, p. 317.
4. Mashchenko, S.Ya. and Silich, S.A., *Numerical Simulations in Astrophysics*, Franco, J., Lizano, S., Aguilar, L., and Daltabuit, E., Eds., Cambridge: Cambridge Univ. Press, 1994, p. 202.
5. Mashchenko, S.Ya. and Silich, S.A., *Astron. Zh.*, 1994, vol. 71, p. 237.
6. Mashchenko, S.Ya. and Silich, S.A., *Astron. Zh.*, 1995, vol. 72, p. 660.

7. Silich, S.A., Mashchenko, S.Ya., Tenorio-Tagle, G., and Franco, J., *Mon. Not. R. Astron. Soc.*, 1996, vol. 280, p. 711.
8. Imshennik, V.S., *Chislennye metody v fizike plazmy* (Numerical Methods in Plasma Physics), Moscow: Nauka, 1977.
9. Bisnovatyi-Kogan, G.S. and Silich, S.A., *Rev. Mod. Phys.*, 1995, vol. 67, p. 661.
10. Brinks, E. and Bajaja, E., *Astron. Astrophys.*, 1986, vol. 169, p. 14.
11. Deul, E.R. and den Hartog, R.H., *Astron. Astrophys.*, 1990, vol. 229, p. 362.
12. Puche, D., Westpfahl, D., Brinks, E., and Roy, J.-R., *Astron. J.*, 1992, vol. 103, p. 1841.
13. Spitzer, L., Jr., *Physical Processes in the Interstellar Medium*, New York: Wiley-Interscience, 1978.
14. Deul, E.R. and van der Hulst, J.M., *Astron. Astrophys., Suppl. Ser.*, 1987, vol. 67, p. 509.
15. Unwin, S.C., *Mon. Not. R. Astron. Soc.*, 1983, vol. 205, p. 773.
16. Brinks, E. and Burton, W.B., *Astron. Astrophys.*, 1984, vol. 141, p. 195.

Translated by D. Gabuzda